

Resonant coupling of electrons and excitons in an aperiodic superlattice under electric fields studied by photoluminescence spectroscopy

S. M. Cao and M. Willander

Department of Physics and Measurement Technology, Linköping Institute of Technology, S-581 83 Linköping, Sweden

A. A. Toropov, T. V. Shubina, B. Ya. Mel'tser, S. V. Shaposhnikov, and P. S. Kop'ev
A.F. Ioffe Physico-Technical Institute, 194021 St. Petersburg, Russia

P. O. Holtz, J. P. Bergman, and B. Monemar

Department of Physics and Measurement Technology, University of Linköping, S-581 83 Linköping, Sweden

(Received 9 March 1995)

We report on a low-temperature (2 K) photoluminescence (PL) investigation of a nine-quantum-well $\text{Al}_{0.4}\text{Ga}_{0.6}\text{As}/\text{GaAs}$ aperiodic superlattice designed to obtain an electron quasiminiband in a desired electric field. The field dependence of the photoluminescence excitation spectra exhibits triple resonance of exciton states originally confined in three neighboring quantum wells and enhancement of the lowest energy exciton intensity due to localizing Coulomb interaction. In the vicinity of a field corresponding to the formation of the quasiminiband, we also observed a drastic quenching of the integrated PL intensity attributed to the fast carrier (electrons) escape through the high-mobility channel formed in the conduction miniband. A comparison of experimental results with numerical calculations of the exciton oscillator strength confirmed that exciton resonance occurred between strongly coupled Stark ladder states.

Heterojunction superlattices (SL's), which consist of periodic quantum wells (QW's) separated by thin potential barriers of a fixed width, have attracted a great interest in recent years.¹ The strong coupling between spatially distributed eigenstates results in unique quantum phenomena such as miniband formation and Wannier-Stark localization, while in the presence of an increasing electric field, decoupling of states transforms the miniband into a Stark ladder and eventually leads to two-dimensional (2D) subbands.²⁻⁸ In a practical device, such a regular SL (RSL) offers a good carrier transport along the growth direction at the cost of a smooth onset of optical absorption. Since the optical transition energies and exciton oscillator strengths (OS's) can be modulated by controlling the interwell coupling strengths, it is possible to design alloy structures which allow both pronounced optical and dynamic transport characteristics in an external field, e.g., compositionally graded SL.^{9,10} One of the approaches can be an aperiodic superlattice (ASL) in which, in contrast to RSL's with fixed QW and barrier widths, sequential QW's and barriers are grown with variational widths, such that in a critical field the spatially confined QW states are recoupled to form extended states. RSL's can also serve to enhance the characteristics of tunneling devices compared with conventional double-barrier resonant tunneling devices.^{11,12} Tunneling in these devices is achieved by incoherent relaxation between two subbands. One step further, we investigate the possibility of a coherent multibarrier tunneling structure using an ASL. Such structures can be of interest for potential applications in optoelectronic devices.

In this paper, we have studied coherent properties of electrons and excitons in an ASL by photoluminescence (PL) spectroscopy at low temperature. We bear in mind that the electron wave function can be coherent throughout the entire ASL in contrast to excitons which cannot be fully extended

due to localization induced by Coulomb interaction.¹³ We designed a finite ASL which has a number of discrete confined subbands at zero field, while at a critical field F_c all the states are aligned in energy and so form a quasiminiband.¹⁴ By approaching F_c , we expect the PL excitation (PLE) spectra to reveal both resonances of the Stark ladder and elimination of the continuum spectrum to a degree suggesting the electron tunneling escape time to be much shorter than other characteristic time scales.

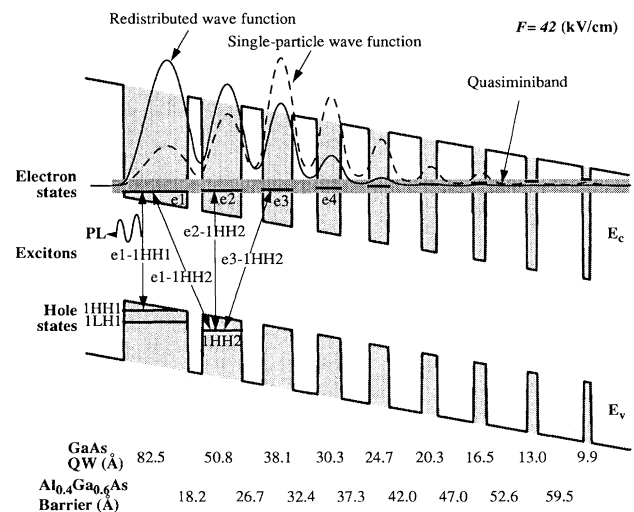


FIG. 1. A schematic view of conduction (E_c) and valence band (E_v) profiles in the ASL under the electric field F . The QW and barrier dimensions are listed below. The single-particle wave function is associated with the lowest energy electron state ($e1$), while the redistributed wave function is the electron distribution in the $e1$ -1HH1 exciton.

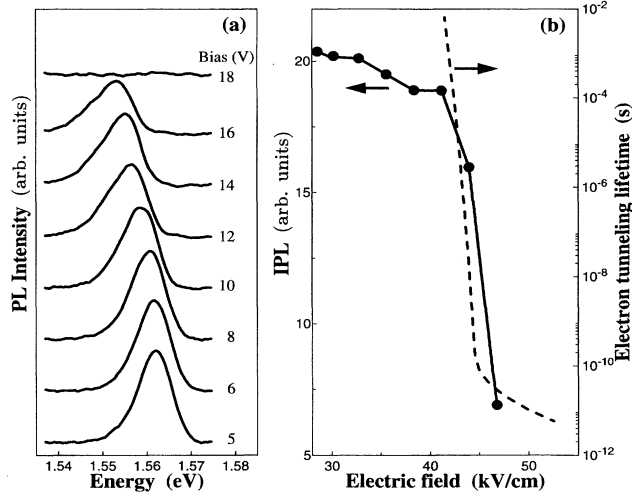


FIG. 2. (a) A series of PL spectra recorded with 15 mW/mm² laser excitation at 7500 Å for different bias voltages at 2 K. (b) Plots of the measured integrated PL intensity (dots) and the calculated electron tunneling time (dashed line) vs electric field.

The sample described in this work was realized in a heterojunction *p-i-n* diode grown by molecular-beam epitaxy on an *n*⁺-type GaAs(100) substrate. A semitransparent gold contact was used to allow optical excitation and to apply bias. A nine-“period” Al_{0.4}Ga_{0.6}As/GaAs ASL (Fig. 1), in which the QW thickness increases and the barrier thickness decreases in the growth direction, was embedded in the center of the 0.94 μm thick *i* region. The ASL conduction band profile is designed in such a way that transfer integrals (TI) of the electron envelope functions in the nearest neighbor QW’s take the same value.¹⁴ Here the TI can be expressed as

$$I_{n,n\pm 1} = \langle \psi_n | \hat{V}_n | \psi_{n\pm 1} \rangle, \quad (1)$$

where ψ_n and \hat{V}_n are the normalized wave function and potential profile for the *n*th single QW, respectively. $I_{n,n\pm 1}$ gives the coupling strength between the states confined in the *n*th QW and in its nearest neighbor. The width of the electron quasiminiband formed at 40 kV/cm is designed to be $4I_{n,n\pm 1} = 24$ meV, while the hole states are decoupled.

Both PL and PLE spectra were measured at 2 K using an optical cryostat operated with liquid He. The optical excitation was obtained from a tunable titanium sapphire solid-state laser at a power of ~15 mW/mm². For PL measurements, an excitation wavelength of 7500 Å was used. For PLE measurements, the detection energy was adjusted for each applied bias in response to the field-induced shift of the PL output. The PL signal was dispersed by a double monochromator (SPEX) and detected by a GaAs photomultiplier tube.

Figure 2(a) shows the PL spectra for serial reverse biases (defined as $U > 0$) applied to the sample. Only one PL peak is evident for each bias originating from the exciton recombination associated with the lowest electron (*e*1) and the lowest heavy-hole states (first HH state in the first QW), i.e., *e*1-1HH1 (see Fig. 1). Transitions from higher states were not observed at this low temperature. It is also noticed that

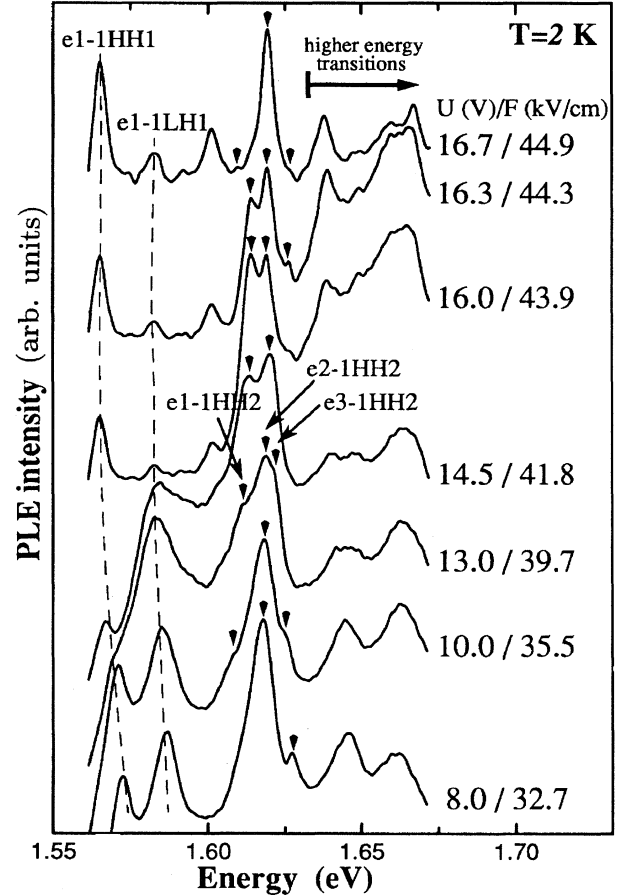


FIG. 3. Normalized PLE spectra in a series of fields measured with 15 mW/mm² laser excitation at 2 K. The field-induced triple resonance between strongly coupled QW states is depicted. The triangles (▼) mark the peak energies of the 1HH2 associated excitons at resonance.

the PL intensity decreases and the linewidth broadens as the bias is increased. Shown in Fig. 2(b), the integrated PL (IPL) intensity drops drastically, when the bias exceeds 14 V (~41 kV/cm), to almost background signal level at 18 V. Generally, two explanations can be applied: the reduction of delocalized exciton OS and the reduction of the electron tunneling escape time¹⁵ from the widest QW (dashed line). We suggest the latter to be more important, since the redshift of the PL energy is clearly attributed to the quantum confined Stark effect associated with a localized exciton state. In fact, resonant quenching of the PL is achieved when approaching the F_c field. This is further supported by examining the field dependence of the PLE spectra.

Figure 3 shows a selected part of PLE spectra in a series of biases applied to the sample. In order to examine the behavior of relative redistribution of exciton peaks, the amplitudes of the PLE spectra have been normalized by the corresponding IPL. The available range of the laser excitation enabled us to detect the excitonic features related to the four widest QW’s. To avoid complications due to overlapping of the HH and LH exciton peaks, we restrict ourselves to discuss transitions involving 1HH1 and 1HH2 states. The 1HH1 associated lowest energy transition is of particular interest since it was involved in the emission process of Fig.

2(a). As the 1HH2 associated exciton peaks are separated from the LH peaks, it is most convenient for us to analyze their energies and to study the Stark ladder resonances near F_c . By calculations partly shown in Fig. 4, we know the link between the external bias and the internal electric field, and can identify the peaks in the PLE spectra. The lowest energy peak in Fig. 3 is associated with the $e1$ -1HH1 exciton (redshifted with increasing field) and the third peak (highest intensity at 8 V) corresponds to the $e2$ -1HH2 exciton from the QW2. Accordingly, the second broad peak at low bias originates from contributions of $e1$ to 1LH1 and 2HH1 transitions. The other broad absorption peaks are attributed to higher energy transitions, e.g., $e2$ -1LH2 and $e3$ -1HH3.

Examining the $e1$ -1HH1 intensity in Fig. 3, we notice that it decreases rapidly until ~ 42 kV/cm and then slightly increases at higher fields. This nonmonotonic behavior cannot be explained by calculation of the exciton OS which decreases monotonically up to F_c with increasing field accompanied by a redshift of the peak. According to our calculation, only above F_c the lowest 1HH1 exciton OS should increase accompanied by a blueshift. F_c is about 45 kV/cm according to Fig. 2(b) and Fig. 4. The absence of any blueshift of the $e1$ -1HH1 peaks in Fig. 3 also confirms that all spectra are measured in fields $\leq F_c$. This contradiction can be understood qualitatively in terms of the transport properties of the ASL and Coulomb-interaction-induced localization of resonantly excited carriers. As compared to the absorption spectra, PLE spectra reflect both absorption coefficient and excitation transfer along the structure, particularly in a SL. In the vicinity of F_c , a one-side open quasiminiband is formed in the conduction band, resulting in an extremely short electron tunneling lifetime which can be as short as a few picoseconds according to our calculations [Fig. 2(b)]. If the electron escape time is shorter than the characteristic time scale of exciton formation and recombination, the contribution from the continuum spectra will be eliminated leading to a fast quenching of the total PL output. The series of spectra in Fig. 3 illustrate the efficiency of this process. When exciting the lowest exciton resonantly, the Coulomb interaction gives rise to localization of the created excitons near QW1 in which 1HH1 is completely confined in a high field. The significance of this localization is illustrated in Fig. 1 where the single-particle wave function of the $e1$ state and the electron wave function (redistributed) in the lowest 1HH1 exciton state are calculated for 42 kV/cm. Thus the Coulomb-interaction-induced localization enhances the lowest exciton binding energy and prevents fast tunneling escape of electrons. In addition, the resonantly created exciton experiences localization due to the heterojunction imperfections and recombines radiatively contributing to the intensity detected in the PLE spectrum. Due to resonance coupling of the electron Stark ladder in an increasing field below F_c , intensity enhancement of the higher energy peaks becomes very abrupt (41.8–44.3 kV/cm). When the applied field reaches F_c , electron tunneling through the formed quasiminiband becomes a dominant factor, which eliminates the continuum PLE spectra, leaving purely excitonic spectra of resonant excitation.

Strong coupling between the electron Stark ladder states should lead to anticrossing and resonance effects observable in the PLE spectra. Indeed, we have identified a triple reso-

nance of the 1HH2 associated excitons (Fig. 3) which has been fitted by the theoretical calculation (Fig. 4) in terms of energies and OS's. In a field of 32.7 kV/cm, the high and low energy peaks are associated with the $e2$ -1HH2 and $e3$ -1HH2 excitons, respectively. The dominant intensity of $e2$ -1HH2 reflects the large overlap between the wave functions of $e2$ and 1HH2 states that in turn results in a strong OS and absorption. The weakness of the $e3$ -1HH2 intensity features the small penetration of the $e3$ wave function into QW2. The $e1$ -1HH2 exciton can be identified at 35.5 kV/cm. At higher field, both the $e1$ -1HH2 and the $e3$ -1HH2 approach the $e2$ -1HH2, indicating the continuous alignment of the quantized states. In the vicinity of F_c , two of the peaks have comparable intensity, and then diverge with noticeable intensity reduction. This triple resonance behavior is a consequence of field-induced mixing and anticrossing between electron states *initially* localized in three neighboring QW's in the ASL.

We have calculated HH and LH exciton energies and OS's in the ASL employing both the 1D Schrödinger equation and the tight-binding methods, which achieved very similar results. Our calculation scheme follows Ref. 14 taking into account both mixing of the Stark ladder states and the quantum confined Stark effect. For clarity, only results for the 1HH2 associated excitons are shown in Fig. 4 compared with the PLE peak energies (crosses) of the aforementioned triple resonance. Our calculation is based on an eight-QW profile, since the thinnest QW9 does not exhibit a good confinement and is separated by a thick barrier (60 Å) from the rest of the ASL. In the intrinsic ASL domain, the field F is assumed to be linear in response to the bias U . The field is fitted using $F = F_0 + fU$, where the built-in field $F_0 = 21.5$ kV/cm, $f = 1.4 \times 10^3$ cm $^{-1}$, and the material thickness is within 2 ML of the nominal value. The material parameters used in our calculations follow commonly accepted values.^{16,17} The good agreement between the calculated results and the ex-

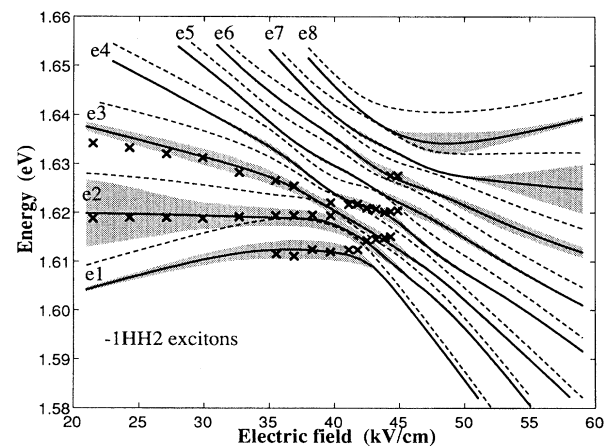


FIG. 4. Plots of the resolved peak energies of 1HH2 excitons (crosses) and the calculated 1HH2 exciton transition energies (lines) vs field. The plot reveals the multiple anticrossing of the 1HH2 associated excitons in the presence of a field. The gray linewidth surrounding the lines is drawn proportional to the corresponding exciton OS. Dashed lines show the sum of the single-particle electron, HH, and band gap energies as a reference.

perimental data in a broad range of fields is encouraging for our understanding of the ASL structure. It is clearly seen that mixing of at least six exciton states (labeled as $e1-e6$) should be taken into account to calculate the excitonic spectrum near F_c . However, the resonance was resolved between strongly coupled states. This confirms that exciton states are also quite extended at the field associated with the formation of the electron quasiminiband.

In summary, we have designed a nine-QW $\text{Al}_{0.4}\text{Ga}_{0.6}\text{As}/\text{GaAs}$ ASL obtaining a conduction quasiminiband in an electric field, which originates from recoupling between multiple QW's. The field dependence of the PL and

PLE intensities confirms the formation of the quasiminiband which efficiently transports photoexcited carriers in the growth direction and significantly reduces the detected PL intensity. A triple resonance is resolved in the PLE spectra associated with the HH exciton transitions, manifesting the importance of coupling of excitonic states for optical response in ASL structures. We have demonstrated the applicability of such an elaborately designed ASL achieving control of both optical and transport properties in desired finite electric fields.

This research was partly supported by the Russian Fundamental Science Foundation Grant No. 94-02-06411a.

-
- ¹F. Agulló-Rueda, J. A. Brum, E. E. Mendez, and J. M. Hong, *Phys. Rev. B* **41**, 1676 (1990), and references therein.
- ²E. E. Mendez, F. Agulló-Rueda, and J. M. Hong, *Phys. Rev. Lett.* **60**, 2426 (1988).
- ³E. E. Mendez and F. Agulló-Rueda, *J. Lumin.* **44**, 223 (1989).
- ⁴R. P. Lavitt and J. W. Little, *Phys. Rev. B* **41**, 5174 (1990).
- ⁵M. Nakayama, I. Tanaka, H. Nishimura, K. Kawashima, and K. Fujiwara, *Phys. Rev. B* **44**, 5935 (1991).
- ⁶P. Roussignol, A. Vinattieri, L. Carraresi, M. Colocci, and A. Fasolino, *Phys. Rev. B* **44**, 8873 (1991).
- ⁷Y. Tokuda, K. Kanamoto, Y. Abe, and N. Tsukada, *Phys. Rev. B* **43**, 7170 (1991).
- ⁸S. Fafard, Y. H. Zhang, and J. L. Merz, *Phys. Rev. B* **48**, 12 308 (1993).
- ⁹F. Agulló-Rueda, H. T. Grahn, A. Fischer, and K. Ploog, *Phys. Rev. B* **45**, 8818 (1992).
- ¹⁰H. T. Grahn, F. Agulló-Rueda, A. D'Intino, K. H. Schmidt, G. H. Döhler, and K. Ploog, *Solid State Electron.* **37**, 835 (1994).
- ¹¹D. Bertram, H. Lage, H. T. Grahn, and K. Ploog, *Appl. Phys. Lett.* **64**, 1012 (1994).
- ¹²H. Schneider, J. Wagner, and K. Ploog, *Phys. Rev. B* **48**, 11 051 (1993).
- ¹³A. M. Fox, D. A. B. Miller, J. E. Cunningham, W. Y. Jan, C. Y. P. Chao, and S. L. Chuang, *Phys. Rev. B* **46**, 15 365 (1992).
- ¹⁴S. M. Cao, M. Willander, E. L. Ivchenko, A. I. Nesvizhskii, and A. A. Toropov, *Superlatt. Microstruct.* **17**, 97 (1995).
- ¹⁵E. J. Austin and M. Jaros, *J. Phys. C* **19**, 533 (1986).
- ¹⁶The parameters for $\text{Al}_x\text{Ga}_{1-x}\text{As}$ material used in the calculation throughout the paper are as follows: electron effective mass $m_e^*/m_0=0.0667+0.0835x$; heavy-hole effective mass $m_{hh}^*/m_0=0.340+0.412x$; light-hole effective mass $m_{lh}^*/m_0=0.094+0.056x$; transverse exciton reduced masses are calculated from Luttinger parameters, heavy- and light-hole masses; band gap discontinuity $\Delta E=1.425x-0.9x^2+1.1x^3$ eV with 60% offset in conduction band, where m_0 is the free-electron mass. The band gap energy is taken as 1.5192 eV for GaAs at 2 K.
- ¹⁷D. A. Broido and L. J. Sham, *Phys. Rev. B* **34**, 3917 (1986).